

# Radial and axial segregation of granular matter in a rotating cylinder: A simulation study

D. C. Rapaport\*

*Physics Department, Bar-Ilan University, Ramat-Gan 52900, Israel*

(Dated: December 26, 2006)

The phenomena of radial and axial segregation in a horizontal rotating cylinder containing a mixture of granular particles of two different species have been modeled using discrete particle simulation. Space-time plots and detailed imagery provide a comprehensive description of what occurs in the system. As is the case experimentally, the nature of the segregation depends on the parameters defining the problem; the radial component of the segregation may be transient or long-lasting, and the axial component may or may not develop. Simulations displaying the different kinds of behavior are described and the particle dynamics associated with the axially segregated state examined. The importance of an appropriate choice of interaction for representing the effective friction force is demonstrated.

PACS numbers: 45.70.Mg, 45.70.Qj, 64.75.+g, 02.70.Ns

## I. INTRODUCTION

The mechanisms responsible for some of the more surprising features of granular matter continue to challenge understanding. In view of the fact that the behavior encountered often differs strongly from systems governed by statistical mechanics and thermodynamics, there is little by way of intuitive help from such theories in trying to understand granular matter, both at rest and in motion. Segregation is perhaps the most prominent of these features; the ability of noncohesive granular mixtures to segregate into individual species, despite the absence of any obvious entropic or energetic benefit, makes this a particularly fascinating phenomenon.

Granular separation and mixing are central to many kinds of industrial processing that span a broad range of size scales; the capability for either causing or preventing segregation can be central to the viability of a particular process. Substantial economic benefits could be gained from a systematic understanding of the complexities of granular flow at a level similar to fluid dynamics; the outcome would be improved control, reliability and efficiency, a notable advance over currently used approaches that are often empirical. Analogous segregation processes occur in nature, where an understanding of the underlying mechanisms might benefit resource management. Consequently, considerable effort has been invested in exploring these phenomena, but, absent a general theory of granular matter, much of the progress in this field [1, 2, 3, 4] relies on computer simulation.

There are a variety of conditions under which granular mixtures segregate; these include shear [5, 6], vibration [7, 8, 9] and rotation [10, 11, 12]. Experiments on rotational segregation, one of the more extensively studied systems experimentally and the subject of the present paper, employ a horizontal cylinder revolving at constant

rate and partially filled with a mixture of two species of granular particles. Given the appropriate kinds of particles, and under suitable conditions, the mixture spontaneously segregates into axial bands of alternating composition. A substantial body of experimental data has been assembled, but because of the numerous parameters entering the experiment only a limited portion of the multidimensional phase diagram has been explored. The relevant parameters include the nature of the granular particles themselves, ranging from the most familiar forms of granular matter such as sand, through various organic products, plastic and glass beads, to metal ball bearings. The particles have a broad spectrum of elastic and frictional characteristics, and sizes that range over several orders of magnitude. The material can be in a dry or wet state, the latter case known as a slurry. The cylinder can have different shapes, most commonly one with a uniform circular cross section. Further parameters include the cylinder diameter and length, the rotation rate, the relative fractions and sizes of the granular components, and the filling level of the container. In marked distinction to fluid systems, there are no known scaling relations that allow this parameter space to be reduced, and while some systematic trends have been noted, there is little guidance available for predicting the outcome of an experiment involving some unexplored combination of parameters.

The most direct observations address the structure of the upper surface [11], while more elaborate studies examine the interior using, for example, noninvasive magnetic resonance imaging (MRI) [13, 14, 15]. Axial segregation may be complete, with each band composed exclusively of one particle species, or it may be only partial, with bands characterized by higher concentrations of alternating species. There is an additional effect that occurs entirely beneath the surface leaving little external evidence, namely radial segregation, which produces a core rich in small particles extending along the length of the cylinder. Radial segregation occurs early in experiments starting from a uniformly mixed state, and may

---

\*Electronic address: rapaport@mail.biu.ac.il

or may not persist once axial segregation appears. Axial band formation might be regarded as a consequence of this core intermittently bulging by an amount sufficient to reach the outer surface [14]. The axial band patterns can also exhibit time dependence; examples of such behavior involve coarsening, in which narrower bands gradually merge into broader bands [16], and the appearance of traveling wave patterns on the surface [17, 18]. Further discussion of the experimental history appears in [12, 14, 19], but information about this phenomenon still continues to accumulate. More recent results showing the richness of the segregation effect and its dynamics in dry and/or wet mixtures (slurries exhibit behavior that is similar in many respects, despite the lubricating role of the fluid medium) are described in [20, 21, 22]. The problem can be extended in different directions, for example [23] considers mixtures with three and more granular components. That there is little opportunity for scaling to play a role in understanding this phenomenon is demonstrated in [24], where the ratio of the cylinder and particle diameters determines whether axial segregation occurs and if its appearance depends reversibly on rotation rate; the fact that the wavelength of the axial pattern does not scale with cylinder diameter is described in [25].

Given the complexity of the experimental situation and the many lacunae in parameter space, it is hardly surprising that theoretical progress has been limited. Continuous one-dimensional models have been developed [26] in which the dynamical variables are the local concentration difference and the slope of the free surface; these describe the early stages of segregation with traveling bands and subsequent band merging, although experiment [27] has questioned their ability to characterize the process correctly, and the obviously important three-dimensional aspects of the phenomenon are absent. The problem has also been studied using a cellular automata approach based on a highly simplified model [28].

The most detailed theoretical approach involves direct modeling of the dynamics of granular particles, employing the same computational methods used in molecular dynamics simulation of atomistic systems. While there have been a considerable number of such studies, covering a variety of granular phenomena, there have been very few simulations of granular particles in a revolving cylinder exhibiting axial segregation. The first of these was an early, rather limited treatment [29]. This was followed by a broader study [12], that is extended by the present work, in which the formation of multiple axial bands was demonstrated, and various aspects of the segregation phenomenon, such as band merging, the absence of mixing in presegregated systems, and the manner in which the behavior depended on the choice of parameters, were investigated. The model differed from that of the present paper in that the transverse restoring force (discussed in detail below) was absent and a Lennard-Jones type of normal repulsion was used rather than a linear force. Exactly the same kind of axial band for-

mation was subsequently reported in [30] (although this similarity was not explicitly noted) using the same kind of model, but with the linear force. The appearance of radial segregation is described in [31], but only for a two-dimensional system.

The purpose of the present paper is to analyze a discrete-particle model that exhibits both axial and radial segregation, in which the appearance of the radial effect precedes the axial, and then either disappears or persists as an axial core. Experimentally, it is the smaller particles that are found to congregate in the interior, and this feature is reproduced by the simulations; one issue that was not resolved in the earlier study [12] was the fact that the opposite behavior was encountered, but it will be shown that this is due to the choice of interparticle forces. The goal here is not a systematic coverage of parameter space, since the computational resources for this would be considerable, but rather a demonstration of the typical kinds of outcome with just a few examples of parameter dependence; indeed, due to a lack of detailed reproducibility under different initial conditions, as will become apparent subsequently, obtaining a comprehensive picture of the “average” behavior would require multiple simulation runs for each parameter set. Typically, the majority of runs described here involve larger systems than before, with a bigger particle size difference and a more slowly rotating cylinder; these changes, together with the additional work required by the force computations, called for a greater computational effort than previously.

## II. SIMULATION METHODOLOGY

### A. Granular models

The models used for granular simulation are generally based on spherical particles whose resistance to overlap is expressed in terms of a continuous potential function [5, 32, 33]. In addition to this excluded-volume repulsion, particles are subject to forces that aim to replicate the effects of inelasticity and friction. There are limitations to the accuracy of such models, with one empirical measure of success being the degree to which the essence of the phenomenon under study is captured.

Consider a pair of granular particles  $i$  and  $j$  with diameters  $d_i$  and  $d_j$ , respectively. The repulsive force between particles depends linearly on their overlap,

$$\mathbf{f}_v = k_n (d_{ij} - r_{ij}) \hat{\mathbf{r}}_{ij}, \quad r_{ij} < d_{ij}, \quad (1)$$

where  $\mathbf{r}_{ij} = \mathbf{r}_i - \mathbf{r}_j$  is the particle separation,  $r_{ij} = |\mathbf{r}_{ij}|$ , and  $d_{ij} = (d_i + d_j)/2$  is the effective diameter. An alternative is the Hertz interaction that depends on the 3/2-power of the overlap [34], whereas in [12] the repulsive part of the Lennard-Jones interaction was used. Dissipative forces act for the duration of each collision. The first of these is velocity-dependent damping along the line

between particle centers,

$$\mathbf{f}_d = -\gamma_n(\hat{\mathbf{r}}_{ij} \cdot \mathbf{v}_{ij})\hat{\mathbf{r}}_{ij}, \quad (2)$$

that depends on the component of relative velocity  $\mathbf{v}_{ij} = \mathbf{v}_i - \mathbf{v}_j$  parallel to  $\mathbf{r}_{ij}$ . Here,  $\gamma_n$  is the normal damping coefficient, assumed to be the same for all particles. The total normal force between particles is then  $\mathbf{f}_n = \mathbf{f}_v + \mathbf{f}_d$ .

Frictional damping acts transversely at the point of contact to oppose sliding while particles are within interaction range,

$$\mathbf{f}_s = -\min(\gamma_s^{c_i c_j} |\mathbf{v}_{ij}^s|, \mu^{c_i c_j} |\mathbf{f}_n|) \hat{\mathbf{v}}_{ij}^s, \quad (3)$$

where the relative transverse velocity of the particle surfaces at this point, allowing for particle rotation, is

$$\mathbf{v}_{ij}^s = \mathbf{v}_{ij} - (\hat{\mathbf{r}}_{ij} \cdot \mathbf{v}_{ij})\hat{\mathbf{r}}_{ij} - \left( \frac{d_i \boldsymbol{\omega}_i + d_j \boldsymbol{\omega}_j}{d_i + d_j} \right) \times \mathbf{r}_{ij}, \quad (4)$$

and  $\boldsymbol{\omega}_i$  is the particle angular velocity. The value of  $\gamma_s^{c_i c_j}$  depends on the particle types  $c_i$  and  $c_j$ , and  $\mu^{c_i c_j}$  is the static friction coefficient that limits the transverse force to a value dependent on  $|\mathbf{f}_n|$ .

In a model of this type there is no true static friction, a practical consequence of which would be stick-slip motion. A way of at least partially overcoming this limitation, though not strictly a correct means of incorporating the effect, is to introduce a tangential restoring force that acts during the collision and depends on the cumulative relative displacement at the point of contact [5, 31, 32]. This force has the form  $\mathbf{f}_g = -k_g \mathbf{u}_{ij}$ , where

$$\mathbf{u}_{ij} = \int_{(\text{coll})} \mathbf{v}_{ij}^s(\tau) d\tau \quad (5)$$

is evaluated as a sum of vector displacements over the interval the particles have been in contact; the magnitude of  $\mathbf{f}_g$  is also limited by  $\mu^{c_i c_j} |\mathbf{f}_n|$ . In addition, to avoid occasional unrealistically large displacements (although this does not appear to affect the behavior), if  $|\mathbf{u}_{ij}| > 0.1$ , an arbitrarily chosen limit, it is reset to zero (a form of ratcheting intuitively motivated by the asperities responsible for friction); an alternative treatment appears in [35]. This history-dependent force was not present in [12]; the results below suggest that it plays an important role in achieving the correct form of radial segregation. The total transverse force is  $\mathbf{f}_t = \mathbf{f}_s + \mathbf{f}_g$ .

The curved cylinder wall and the flat end caps are treated as rough and smooth boundaries respectively. The interaction of particles with the curved boundary (together with gravity) drives the system, so this force includes the same components as the interparticle force. On the other hand, to minimize spurious effects associated with the end caps, only  $\mathbf{f}_v$  and  $\mathbf{f}_d$  act there. Further details concerning the interactions (with the exception of  $\mathbf{f}_g$ ) appear in [12], together with a discussion of the friction coefficients and the particle-wall force computations. Other aspects of the simulation follow standard molecular dynamics procedures [36]; neighbor lists are used to

efficiently organize the force computations, the translational and rotational equations of motion are integrated with the leapfrog method, and parallel processing can improve performance.

## B. Parameters

Those parameters that also appeared in [12] have been assigned similar values here. The first of these is the gravitational acceleration,  $g = 5$ , which then relates the dimensionless MD units used in the simulation to the corresponding physical units. Thus, if  $L_{MD}$  is the length unit (in mm), then the time unit is  $T_{MD} \approx 10^{-2} \sqrt{5L_{MD}}$  s. If the cylinder rotates with angular velocity  $\Omega$  (MD units) the actual rotation rate is  $\Omega/(2\pi T_{MD}) \approx 7.1\Omega/\sqrt{L_{MD}}$  Hz; for 3 mm particles,  $\Omega = 0.1$  is equivalent to 25 rpm, a typical experimental value.

Axial segregation tends to develop slowly, leading to long simulation runs. Computational cost can be reduced by using the largest possible integration time step; the step size  $\delta t$  is limited by the highest particle speeds encountered and here the value used is  $\delta t = 5 \times 10^{-3}$  (MD units). Numerical stability considerations then set a lower bound on the collision time to ensure it remains much larger than  $\delta t$  (typically 30–40×). Collisions between particles in the slowly varying bulk interior can be protracted events, but the opposite is true for particles bouncing rapidly along the upper free surface, and this in turn constrains coefficients such as particle stiffness. For the present work, most runs use  $k_n = 1000$  in Eq. (1). Increasing this to, e.g.,  $10^5$  would require a 10-fold reduction in  $\delta t$  and a much longer computation; however, since there are  $\approx 10^4$  steps/revolution, some runs already exceed  $10^7$  steps, so this is not presently feasible in general.

The relatively small cylinder diameters and fill levels used here (details below) limit the compression forces that particles can experience. At the base of a static column of 10 small particles the overlap (which can be regarded as compression) will be 5% (for  $k_n$  and  $g$  as given), an amount that is unlikely to alter the qualitative behavior; indeed, tangential forces will be enhanced for softer particles that experience a greater number of longer-lasting contacts. (Particles with the  $r^{-12}$  repulsion that is part of the force used in [12] have an overlap three times larger; the ultimately greater resistance of this force to compression asserts itself only at five times the depth.) Systems with substantially thicker layers will require a stiffer volume interaction (and consequently a smaller  $\delta t$ ).

The values of the remaining parameters from [12] are as follows. In Eq. (2),  $\gamma_n = 5$ . The coefficients in Eq. (3) are  $\gamma_s^{bb} = 10$ , and in general  $\gamma_s^{ss} = \gamma_s^{bs} = 2$ , except for a few cases where all  $\gamma_s = 10$ ; the particle-wall values are identical. The relative values of the static friction coefficients, e.g.,  $\mu^{bb}/\mu^{ss}$ , are set equal to the ratio of

the corresponding  $\gamma_s$  values, with the larger of the pair equal to 0.5. Finally, the value of the new parameter introduced with Eq. (5) is  $k_g = 500$ , although, as with most parameter settings, there is considerable latitude, and all that is required at this exploratory stage is for the results to appear qualitatively reasonable.

The nominal particle diameter is the interaction cutoff in Eq. (1). For small particles, to maintain consistency with [12],  $d_s = 2^{1/6} \approx 1.122$  (MD units), while for big particles  $d_b = bd_s$ . The actual particle sizes are uniformly distributed over a narrow range  $[d_s - 0.2, d_s]$  for small particles, and likewise for big; the mean diameter of the small particles is then close to unity. Particles all have the same density, so the big to small mass ratio (before allowing for the random size distribution) is  $b^3$ . The relative population of big and small particles is chosen to give equal volume fractions; for most runs  $b = 1.8$ , with a big particle fraction of 0.15.

The cylinder diameter  $D$  and length  $L$  have value ranges 30–40 and 120–360 (MD units) respectively. (A consequence of the use of soft potentials is that the effective  $D$  and  $L$  values are reduced by approximately one unit.) The aspect ratio  $L/D$ , a quantity having some influence on the number of axial segregation bands [25], lies between 4 and 12. The cylinders used here are relatively narrow, with  $D$  less than 30 times the mean particle diameter, a limitation that has been found experimentally to influence behavior [24]; even so, the number of particles in a simulation can exceed 70 000. Another connection between experiment and simulation is the dimensionless Froude number  $\text{Fr} = \Omega^2 D/2g$ , the ratio of centrifugal to gravitational acceleration. Experimentally  $\text{Fr} \approx 10^{-3}$ – $10^{-1}$ , and to ensure the simulations remain in the correct regime, the value should not be allowed to become too large; this sets an upper limit to  $\Omega$ , and for the simulations  $\text{Fr} < 0.2$ .

### C. Measuring segregation

Quantitative measures of the overall intensity of axial and radial segregation are used to augment direct observation. The time-dependent axial segregation,  $S_a(t)$ , is evaluated from binned counts along the axis weighted by particle mass,

$$S_a = \frac{\langle |b^3 n_b(q) - n_s(q)| \rangle_q}{b^3 n_b + n_s}, \quad (6)$$

where  $n_b(q)$  and  $n_s(q)$  are the number of big and small particles in a slice (width  $\approx 2.5$ ) centered at  $q$  along the axis,  $\langle \dots \rangle_q$  denotes an average over all slices, and  $n_b$  and  $n_s$  are the totals. Binned counts are less suitable for evaluating the radial segregation,  $S_r(t)$ , because, if done in the same way as the space-time plots discussed below, not all particles would be able to contribute. An alternative measure, based on the mean-square radial distance of each type of particle from its center of mass, is therefore

used,

$$S_r = \frac{(\langle r_b^2 \rangle - \langle r_b \rangle^2) - (\langle r_s^2 \rangle - \langle r_s \rangle^2)}{\langle r^2 \rangle - \langle r \rangle^2}, \quad (7)$$

where  $\langle r_b \rangle$  and  $\langle r_s \rangle$  denote the mean distances of big and small particles from the axis, and  $\langle r \rangle$  the overall mean. Time is expressed in terms of the number of cylinder revolutions,  $n_R$ .

## III. RESULTS

Due to the very nature of the segregation effect, not all of its features are readily quantifiable. The functions  $S_a(t)$  and  $S_r(t)$ , Eqs. (6–7), provide a global summary of pattern development, but lack detailed information concerning the number of axial bands, the sharpness of the boundaries between segregated regions and the regularity of the band pattern. The use of space-time plots, coded using either color or grayscale level, provides a much more detailed picture of how both axial and radial segregation evolve with time. Such plots show the relative populations, weighted by particle volumes, in appropriately oriented slices. For the axial plots, slices are normal to the cylinder axis; while this does not provide the same information as the surface populations seen in experiment, it will be similar provided that radial inhomogeneity is weak. For the radial plots, slices are parallel to the upper free surface of the material; the nominal surface slope is determined by a linear fit to the inner 2/3 of the surface away from the curved boundary, and only the particle populations in a slab of similar width normal to the surface are counted, to avoid bias due to the shape of the region.

Even more detailed information can be extracted from snapshots of the entire system, in which particular subsets of particles can be selected for viewing; images of this kind can, for example, reveal interior organization analogous to that observed experimentally with MRI. An even richer visual approach employs animated recordings showing the full temporal development of the system. An animation of this type consists of an extended series of snapshots, recorded at regular intervals throughout the run; all the information needed for the analysis that follows is in fact obtained from configurations reconstructed from such recordings.

The runs described here are cataloged in Table I; they are labeled alphabetically for reference and listed in the order they first appear in the discussion. Run lengths were not specified in advance; a run was generally allowed to continue for as long as something interesting was happening, or until it seemed that the system had stabilized (the possibility of premature termination can never be ruled out), or until changes appeared to be occurring too slowly to warrant continuation.

Most runs are begun from a uniformly mixed initial state, and in a few cases, from a state that is presegregated into two axial bands. The particles are placed

TABLE I: Summary of runs discussed in the text; the top row includes the default settings used unless indicated otherwise.

Id <sup>a</sup>	Size, etc. <sup>b</sup>				M <sup>c</sup>	Forces <sup>d</sup>		R <sup>e</sup>	Outcome					
	L	D	$\rho$	N		b	$\Omega$	$k_n$	$k_g$	$\gamma_s^{ss}$	$n_R$ <sup>f</sup>	Rd <sup>g</sup>		
A	240	40	.30	71 600	1.8	.2	M	1000	500	2	1620	P	12	
B	360	30		57 600		.1					2630	T	17→11	
C	160	40		47 300		.1					1800	P	7	
D	120	30	.50	35 900							470	P	-	
E	120	30		18 800							2940	T	6	
F	120	30		18 800							R	1310	T	5
G	120	30		18 800							R	1310	T	7→4
H	120	30	.40	24 200							730	P	-	
I	120	30	.45	29 300							590	P	-	
J	120	30		18 800		.1					4290	T	6→3	
K	360	30		57 600							2960	T	17→12	
L	160	40		47 300							3320	P	7	
M	120	30		18 800				0			2040	I	3	
N	120	30		18 800				0			R	1030	I	5
O	120	30	.45	29 300				0			830	P	-	
P	120	30		19 200	1.5						6350	-	7→5	
Q	120	30		19 200	1.3						2760	-	6	
R	120	30		18 800			2000				2610	T	6→3	
S	120	30		18 800				10			6350	P	2 <sup>i</sup>	
T	180	30		16 800		S					2840	-	2	
U	180	30		16 800		S					10	2440	P	-
V	160	40	.18	27 900		S					6110	-	2→4	

<sup>a</sup>Runs are denoted in the text as #A, etc.

<sup>b</sup>Cylinder length  $L$  and diameter  $D$ , filling density  $\rho$ , number of particles  $N$  (rounded to nearest 100), big particle size  $b$ , angular velocity  $\Omega$ .

<sup>c</sup>M/S: Mixed or segregated initial state.

<sup>d</sup>Values of force coefficients:  $k_n$ ,  $k_g$  and  $\gamma_s^{ss}$ ; all others are constant with values listed in the text.

<sup>e</sup>R denotes repeat of preceding run with different initial state.

<sup>f</sup>Run length, in cylinder revolutions.

<sup>g</sup>Radial segregation: permanent, transient, inverted, or none.

<sup>h</sup>Axial segregation: initial and final band count, or none.

<sup>i</sup>Partial segregation only.

on a lattice and assigned small random velocities (details that vanish after just a few collisions); particle species is either randomly assigned according to relative concentration, or, in the presegregated case, determined by axial position. A change of random number seed allows repeated runs of systems that are otherwise identical.

In all cases the cylinder is capped at the ends. Use of an axially periodic cylinder leads to similar pattern development, establishing that caps are not required for segregation. However, as in [12], the entire band structure is then subject to axial drift. Since there is no evidence that the caps affect the results (apart from relaxing the requirement for an even number of bands in the periodic case) they can be used without concern.

In view of the extensive simulations involved, it is interesting to consider the computational performance. For a system of 47 000 particles, and a partly parallelized computation running on a dual 3.6 GHz Intel Xeon workstation, the simulation proceeds at a rate of approximately 23 000 time steps/hr, equivalent to 3.7 revolutions/hr at  $\Omega = 0.2$ ; some of the runs therefore extend over several

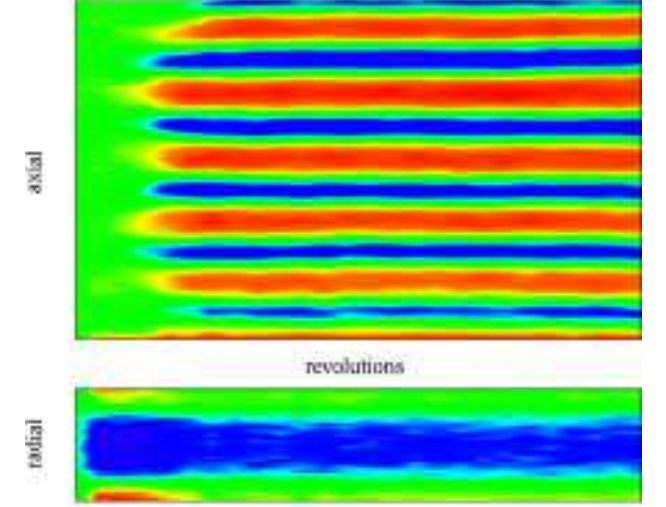


FIG. 1: (Color online) Axial and radial space-time plots for run #A ( $n_R = 1620$ ,  $L = 240$ ,  $L/D = 6$ ); red and blue (or medium and dark gray) denote higher volume fractions of big or small particles. Time, expressed as cylinder revolutions, is along the horizontal axis, and the vertical axis measures axial or radial (the latter normal to the free surface) position.

weeks. Contrast this with a typical experiment that can be run at, e.g., 1000 revolutions/hr, irrespective of the number of particles.

### A. Axial and radial segregation

The first two runs discussed are among the more extensive carried out. While similar in respect to the initial radial segregation that peaks after some 10–20 revolutions and the appearance of multiple axial bands, in one instance radial segregation persists while in the other it practically vanishes. The details of these two runs, #A and #B, will be described using axial and radial space-time plots, together with pictures of the final states that reveal the nature of the internal structure, and with graphs of segregation as measured by  $S_a$  and  $S_r$ . Both runs suggest that a steady final state has been achieved, although, given the experimentally observed long-term slowdown in the bond merging rate, there is no way of completely excluding future changes of this type, no matter how long the run.

Fig. 1 shows the axial and radial space-time plots for run #A. Radial segregation appears very early in the run and a core of small particles persists throughout, although the outer layer rich in big particles disappears from the radial plot once axial banding begins; after the 12 axial bands have formed the pattern appears stable, with no hint of any future change.

Images of the final state of run #A appear in Fig. 2. The first is an oblique view of the full system showing the 12 alternating bands. The others are views looking down in a direction normal to the surface that show big

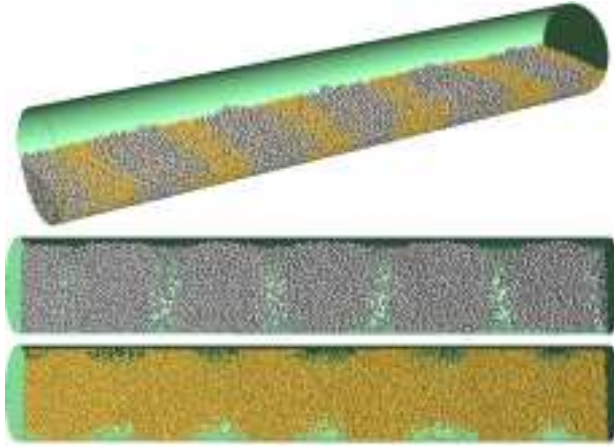


FIG. 2: (Color online) Final state of run  $\#A$ ; the full system, and views showing just the big and small particles (colored silver and gold).

and small particles separately. These interior views reveal that while the bands of big particles are not entirely separate, there are visible divisions between them, and that the bands of small particles are joined by a central core extending the length of the system.

Fig. 3 shows the space-time plots for run  $\#B$ . Here, unlike  $\#A$ , radial segregation is a transient effect lasting less than 200 revolutions; furthermore, the early axial pattern is not maintained, and the initial 17 bands are eventually reduced to 11 due to the vanishing of the small particle bands at the ends and the merging of two pairs of big particle bands (eliminating two more small particle bands). During the latter portion of the run, extending over more than half its total length, there is no suggestion of further pattern change. Band coarsening is a well-known experimental result, with the band count falling roughly logarithmically with time [20], although the dependence can be more complicated than this [22].

The images in Fig. 4 show the final state of  $\#B$ . Band separation is practically complete in this case, with essentially no misplaced big particles, and only the faintest remnant of a small particle core.

The development of axial and radial segregation,  $S_a$  and  $S_r$ , for these two runs is shown in Fig. 5. The graphs reflect what has already been noted in the space-time plots and images, namely, that a preference for small particles in the core persists over the duration of  $\#A$ , but not  $\#B$ ; the presence of this core affects the magnitude of  $S_a$ , which is smaller in  $\#A$  than in  $\#B$ .

The images in the next two figures provide examples of radial segregation in cases where the effect is well developed. Fig. 6 shows  $\#C$  after 60 revolutions; this run eventually develops axial segregation. The complete system is shown, together with three narrow slices (of thickness  $0.03L$ ) at the midpoint and at a distance  $0.1L$  from either end.

Fig. 7 shows  $\#D$  after 260 revolutions (graphs of  $S_a$  and  $S_r$  for this run appear later). The view is along

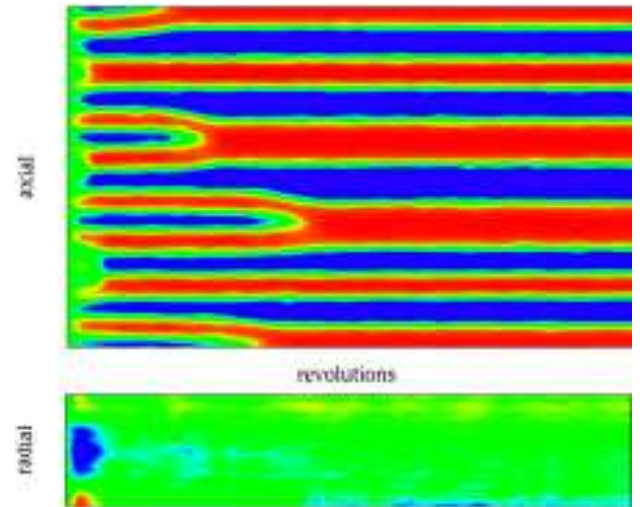


FIG. 3: (Color online) Axial and radial space-time plots for  $\#B$  ( $n_R = 2630$ ,  $L = 360$ ,  $L/D = 12$ ).

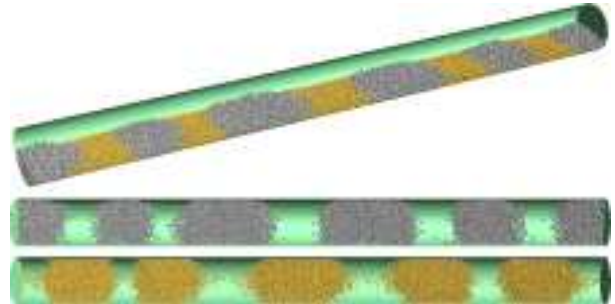


FIG. 4: (Color online) Final state of  $\#B$ .

the axis, after slices of thickness  $0.1L$  are removed from each end; on the left all particles are shown, while on the right just the big particles appear. There is a visible opening extending along the entire length ( $0.8L$ ) near the center of the small particle core; while the simulations do not produce a totally pure core, radial segregation is strong despite misplaced big particles; this rather short run showed no hint of imminent axial segregation.

Two general observations concerning segregation emerge from these (and subsequent) simulation runs. When radial segregation occurs it takes the form of a core of small particles surrounded by big particles (there is an exception that is discussed below); this is also the case experimentally, although in the simulations the core boundaries are not as sharp and the effect appears to develop more slowly. There is no preferred particle type near the end caps nor a tendency for bands to nucleate there; bands can form at different axial positions at different times; sometimes bond formation is almost simultaneous and sometimes not.

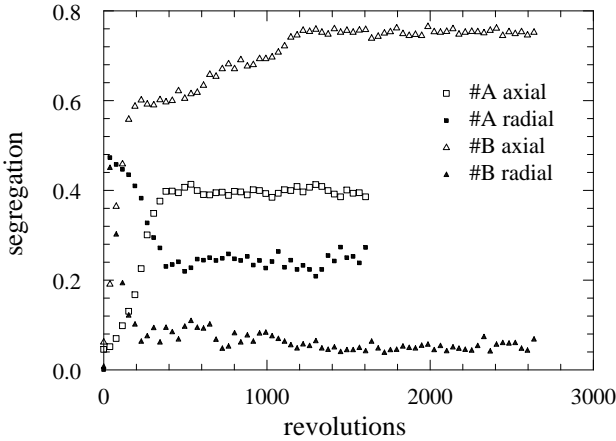


FIG. 5: Time-dependent axial and radial segregation,  $S_a$  and  $S_r$ , for runs  $\#A$  and  $\#B$ ; time is expressed in cylinder revolutions.

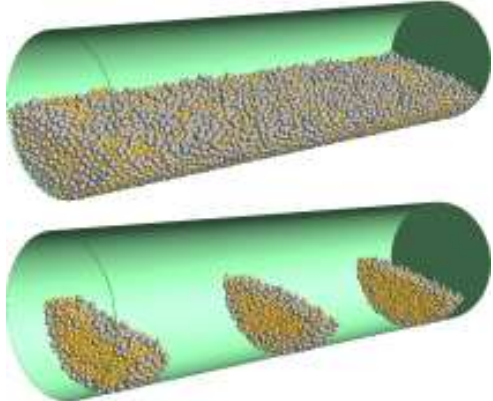


FIG. 6: (Color online) Views of  $\#C$  after 60 revolutions; the full system and three slices are shown.

### B. Reproducibility

The issue of reproducibility is of particular importance since conclusions must take into account the variability of the behavior, such as different intermediate or terminal band counts. Multiple runs would be required, as is normal experimentally. In most cases this condition has

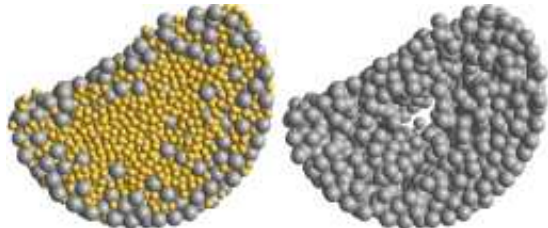


FIG. 7: (Color online) Views of  $\#D$  after 260 revolutions (see text for explanation).

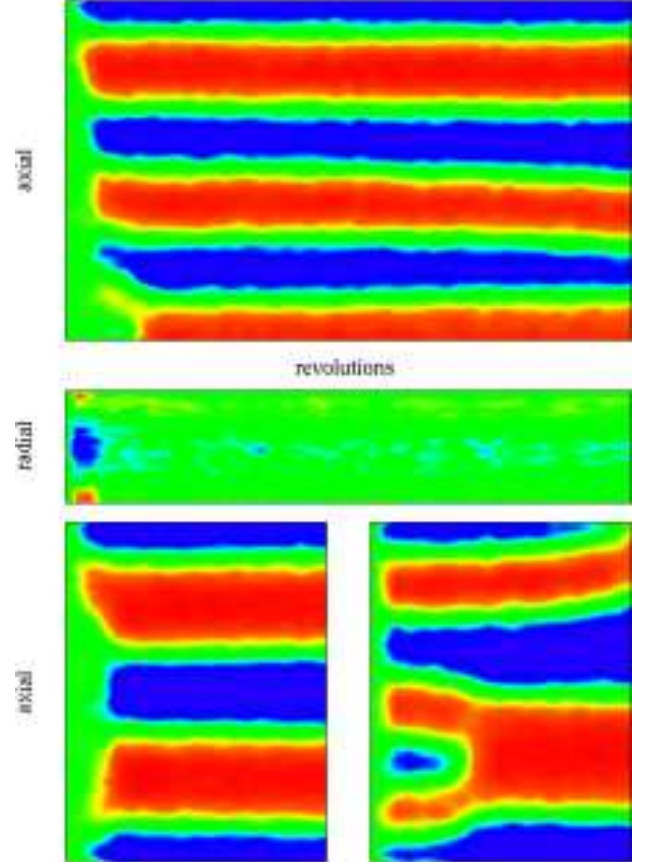


FIG. 8: (Color online) Axial and radial space-time plots for run  $\#E$  ( $n_R = 2940$ ) and, on the same scale, axial plots for  $\#F$  and  $\#G$  ( $n_R = 1310$ ) with different initial states ( $L = 120$ ,  $L/D = 4$ ).

not been fulfilled, but an example of three runs involving systems that are identical, apart from the initial random state, is considered here (and one further example appears later).

Fig. 8 shows the axial and radial space-time plots for run  $\#E$ , together with the axial plots for the shorter runs  $\#F$  and  $\#G$ . The behavior differs (although  $S_a$  and  $S_r$  are only weakly affected); each exhibits early radial segregation, but they differ in regard to axial band development. This is just what happens experimentally under appropriate conditions [20]; some aspects of the segregation ( $S_a$  and  $S_r$ ) are reasonably robust, while others (the band details) may vary significantly between runs. A preferred wavelength governing the axial band pattern could exist, but since development history can influence outcome, it is probably only meaningful to refer to a mean number of bands (and a mean wavelength).

### C. Parameter dependence

When comparing simulation to experiment, the parameters defining the system fall into two categories. There

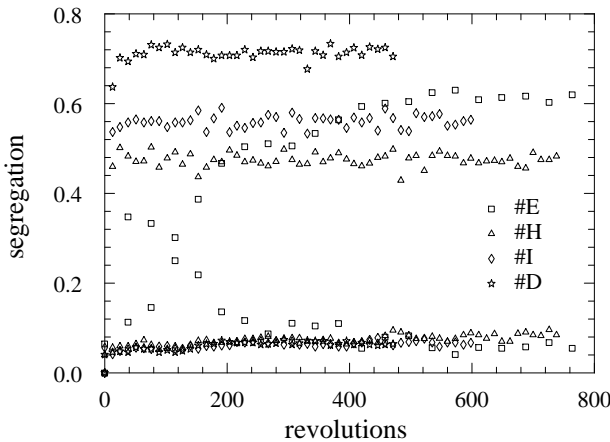


FIG. 9: Axial and radial segregation (the graphs for the latter peak early in each case) for runs  $\#E$ ,  $\#H$ ,  $\#I$  and  $\#D$  with increasing fill level.

are those that are readily changed in an experiment, such as the cylinder rotation rate, the fill level, and even the cylinder size; experimental results may cover a range of these parameters in order to demonstrate trends or construct phase diagrams. The others are related to the properties of the particles themselves; while there are numerous types of granular material available for experimental study, efforts have tended to focus on a rather limited subset, so that a systematic coverage of behavior in terms of material properties is presently unavailable.

Changing the fill level can alter the nature of the segregation, as seen experimentally with slurries [21]. Fig. 9 shows  $S_a$  and  $S_r$  for four runs differing only in their fill level,  $\#E$ ,  $\#H$ ,  $\#I$  and  $\#D$  (because of the slight reduction in effective cylinder size mentioned earlier,  $\rho = 0.45$  corresponds to a cylinder that is approximately half full, while for  $\rho = 0.3$  the layer depth is close to  $\frac{3}{8}D$ ). In  $\#E$ , transient radial segregation is followed by axial, while in the other three cases only radial segregation occurs. These and other runs suggest that a sufficiently high fill level favors permanent radial segregation and at the same time suppresses axial segregation. Validation of the model, and determining how closely it reproduces experiment, requires that behavioral trends under a change of parameters be reproduced correctly; while experiment suggests band suppression at low fill levels [21], this applies to slurries, and the degree of similarity between dry and wet mixtures has yet to be studied systematically.

The cylinder angular velocity  $\Omega$  is the parameter most readily changed in an experiment. The  $\Omega$  dependence (using the values  $\Omega = 0.2$  and  $0.1$ ) for three pairs of runs that are otherwise the same has been examined; the run pairs are  $\#E$  and  $\#J$  that eventually produce 6 and 3 bands,  $\#K$  and  $\#B$  that produce 12 and 11 bands and, lastly,  $\#L$  and  $\#C$  that both produce 7 bands (a tentative result in the case of  $\#C$ ). A feature common to each of these pairs is that  $S_a$  is slightly larger at reduced  $\Omega$ .

The influence of other parameters will be mentioned only briefly. Runs  $\#M$  and  $\#N$  show the effect of removing the tangential restoring force,  $k_g = 0$  in Eq. (5), in a sense making the particles less “grain-like”. The runs are otherwise similar to  $\#E$  and, apart from the function used for  $\mathbf{f}_v$  in Eq. (1), now resemble [12]; so do the results, in which axial segregation is now accompanied by inverse radial segregation. This outcome confirms the importance of  $\mathbf{f}_g$  for obtaining the correct radial behavior. Early in these runs weak normal radial segregation occurs, but it becomes inverted when the axial bands appear. Different behavior is encountered at a higher fill level; run  $\#O$ , which is related to run  $\#I$  in a similar way, shows normal radial but no axial segregation. Outcomes such as these hint at the complex interplay of parameters and call for an extensive coverage, with multiple runs, prior to drawing conclusions.

Another key parameter is  $b$ , the relative size of the big particles. In run  $\#P$ ,  $b$  is reduced to 1.5, and 5 axial bands appear, but no measurable radial segregation;  $b$  is further reduced to 1.3 (the preferred value in [12]) in run  $\#Q$ , resulting in 6 bands. In the opposite direction, it is questionable how large  $b$  can become without having to increase cylinder diameter to avoid serious size effects (and, to maintain aspect ratio, also its length), but for  $b = 2.1$  (not shown), depending on fill level, both radial and axial segregation can be obtained; experiment typically involves  $b \approx 3$  or greater.

Making the particles slightly less compressible by doubling  $k_n$ , in run  $\#R$ , leads to initial radial segregation, and eventually three axial bands. A more substantial increase in  $k_n$  would, as noted earlier, require a smaller  $\delta t$ . Further runs (not shown) similar to  $\#A$ , but with  $k_n$  and all the other interaction coefficients increased by factors of 10 or 100, and with suitably reduced  $\delta t$ , produce the same segregation effects, confirming that this aspect of the model does not significantly influence the behavior. A similar conclusion applies to granular chute flow [35]. For a final example of parameter dependence (requiring further study), run  $\#S$  is similar to  $\#E$  except that  $\gamma_s^{ss} = \gamma_s^{bb} = 10$ ; radial segregation occurs, suggesting that this effect can be driven by particle size difference alone, and eventually two weakly developed axial bands appear (the outcome of this long run is less clear than usual since a final state had yet to develop).

#### D. Particle motion

The configurational snapshots recorded during the runs enable post-run analysis of the motion of individual or selected groups of particles over extended intervals. An eventual goal for this kind of analysis is developing a capability for relating local organization and dynamics at the level of individual particles to the behavior at a scale where the collective nature of segregation is exhibited. Two examples will be considered here.

The first is the merging of two bands of big particles,

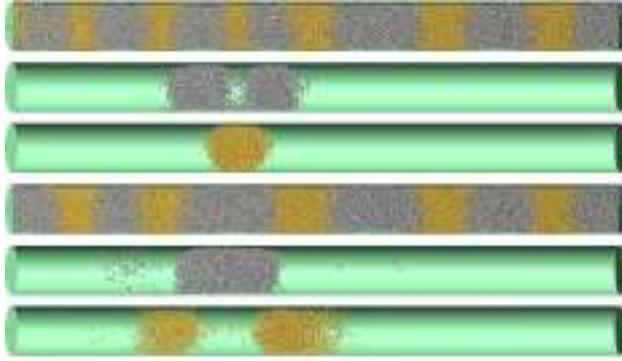


FIG. 10: (Color online) Band merging in run  $\#B$  where small particles from the middle band disperse allowing the big particle bands to merge; the views show the full system and the particles from the bands involved, both before and after the event.

accompanied by the dispersal of the small particles from the disappearing middle band. A merge event of this type occurs in run  $\#B$  (see Fig. 3) between revolutions 700 and 1200. The upper portion of Fig. 10 shows three views prior to the event, namely the full system, and the selected bands of big and small particles (the latter also revealing small particles that intrude into the big particle band, a detail hidden from the outside). The lower portion shows three views at the completion of the event, namely the full system, and all the previously selected particles in their new positions, principally within the bands directly involved. Even though there is essentially no residual small particle core at this stage of the run, small particles are able to migrate across the big particle bands more readily than the converse; selective migration of this kind will be even more apparent in the next example. An interesting feature revealed by these images is that while the small particles are dispersed in both directions, more seem to have traveled to the right where the original band of big particles was somewhat narrower; while such behavior might not be unexpected it is gratifying to see it actually occurring.

The second example also involves run  $\#B$ , but now for monitoring the steady state over a relatively long interval between revolutions 1230 and 2600. The first view in Fig. 11 is of the entire system at the beginning; the next two views show the adjacent, slightly overlapped bands of big and small particles selected for tracking. The last two views show all the selected particles in their final positions (since the band structure is stationary, views of the entire system during the interval are practically indistinguishable); although quite a few small particles (but constituting only a tiny fraction of the band population) have migrated out of the band in both directions, almost no big particles have done likewise, demonstrating that they are effectively confined for lack of an escape path. Departing particles are replaced by others, but these are not shown. This form of analysis can also be carried out experimentally by adding tracer particles to existing

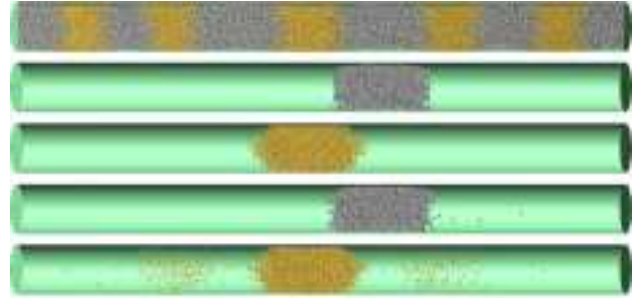


FIG. 11: (Color online) Particle migration and confinement over an interval of almost 1400 revolutions during run  $\#B$ ; the views show the full system at the start of the interval together with the selected bands of big and small particles, and the same sets of big and small particles at the end.

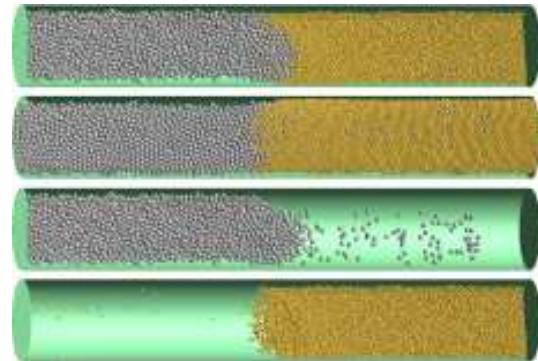


FIG. 12: (Color online) Final state of  $\#T$ ; top, bottom, big and small particle views.

bands [22], revealing that confinement is indeed a strong effect.

### E. Presegregated systems

An alternative perspective is provided by systems that begin in an axially segregated state, a problem also studied experimentally with MRI [22, 37]. Various scenarios exist, of which preserving the original state and axial mixing represent two extremes, while rearrangement into some other band pattern is also a possibility. Examples of all three types will be considered. Very little change occurs over the duration of run  $\#T$ . Fig. 12 shows its final state, and from the top and bottom views it is apparent that the interface has adopted a curved form. The views showing big and small particles separately reveal that comparatively small numbers of each type have penetrated into the opposite region; interestingly, in this example big particles also appear to be participating in the migration.

Mixing is most easily achieved by setting all the friction parameters equal (as in  $\#S$ , where only a weak axial effect was seen). Fig. 13 shows the outcome of this in run  $\#U$ ; the initial axial segregation vanishes promptly

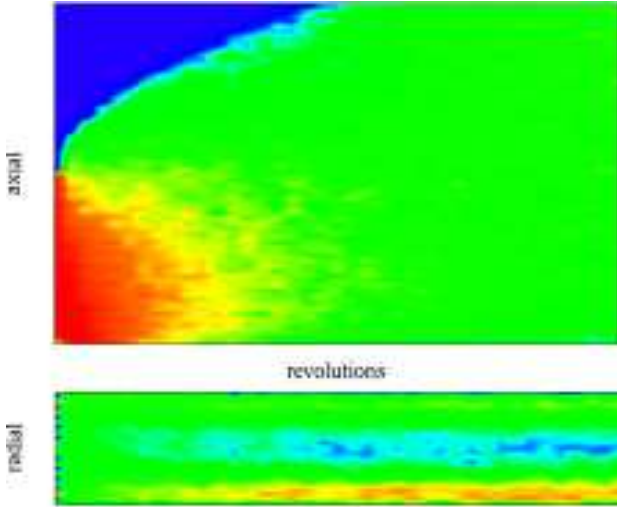


FIG. 13: (Color online) Axial and radial space-time plots for  $\#U$  ( $n_R = 2440$ ,  $L = 180$ ,  $L/D = 6$ ).

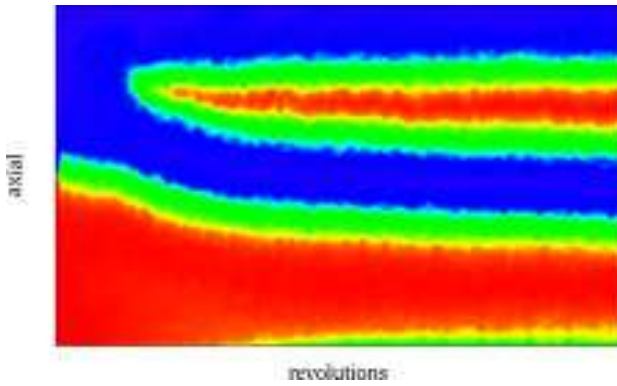


FIG. 14: (Color online) Axial space-time plot for  $\#V$  ( $n_R = 6110$ ,  $L = 160$ ,  $L/D = 4$ ).

and a certain amount of radial segregation appears.

The final scenario, the appearance of an altered axial band pattern, occurs in run  $\#V$  (similar to  $\#L$  but with fewer particles), shown in Fig. 14. The most prominent feature here is the splitting of the small particle band by a new band of big particles. The process involves particle migration in both directions; from the recorded configurations (not shown) it appears that small particles follow an interior path while big particles tend to prefer a path close to the curved cylinder wall; the dynamics of this process is yet another aspect of the overall problem needing further study.

#### F. Surface profiles

The motion of particles along the upper free surface plays a role in the segregation process, although the importance of this contribution and the mechanism involved is open to question. The detailed form of the surface is

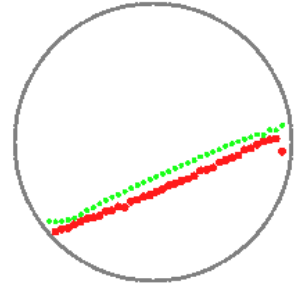


FIG. 15: Averaged surface profiles for big and small particles (big and small points) for run  $\#L$  ( $D = 40$ ).

therefore of interest, although it is not readily characterized and, for a specific particle mixture, it will depend on fill level, rotation rate and cylinder diameter. The profile of the free surface typically varies slightly with position along the axis once axial segregation has occurred. For these reasons, just one instance is included here. Experimental examples, ranging from strongly S-shaped to almost linear, appear in [38].

Fig. 15 shows the axially averaged surface profile near the end of run  $\#L$ , where there are seven bands; big and small particles are treated individually, and the results represent an average over ten configurations spaced six revolutions apart. The profiles are reasonably close to linear (curved profiles similar to [12] can be obtained at lower fill levels); the big particles appear slightly below the small because it is the particle centers that are monitored. There are deviations adjacent to the curved cylinder wall, but here the data binning produces some distortion. Whether the slight deviations from linearity are important for the segregation process remains to be seen. Except at the start, there is no obvious change in this profile over the entire run.

#### IV. CONCLUSION

Simulations based on a simple particle-based model of granular matter have been used to demonstrate the occurrence of both radial and axial segregation in a rotating cylinder containing a two-component granular mixture. The earlier inability to reproduce radial segregation correctly has been resolved; for the type of model considered, this is due to the omission of a component of the frictional force that helps resist sliding during collisions. The different forms of segregation observed are indicative of a large, complex parameter space, as is the case experimentally.

In order to learn more about the phase diagram and determine which parameters dominate in different regimes, a systematic study, including multiple realizations due to reproducibility issues, is required. The results suggest many questions of the “what if” type; of necessity, the answers will also have to await further work. The model

itself is open to critical examination, in particular, how the components of the interparticle force influence the behavior (one example has already been given), as well as the relevant ranges of the force parameters. More generally, in view of the way static friction is represented, how reliable is the model altogether (a question equally applicable to similar models appearing elsewhere)?

In theoretical fluid dynamics, stability analysis [39] is used to determine when symmetry breaking is advantageous. No analogous theory exists for the granular segregation phenomena described here, and the question of what distinguishes the different segregation modes from one another, and from the uniformly mixed state, remains open; is it, for example, the ability to optimize energy dissipation, thereby ensuring the most efficient

flow? The segregation band coarsening slows with increasing band width, and the states eventually reached have varying numbers of bands and degrees of pattern regularity; here the question is whether such patterns are stable, or are they slow transients en route to even further coarsening? Another issue is the relation between the radial and axial segregation processes; are they independent phenomena that just happen to coexist (perhaps in competition) in most, but not all situations, or does the former actually drive the latter? Finally, no attempt has been made to probe the underlying mechanisms beyond the exercises in particle tracking; if simulation can be shown to reproduce experiment reliably, then, in view of the level of detail provided, it may prove an important tool for exploring the complexities of segregation.

---

[1] G. C. Barker, in *Granular Matter: An Interdisciplinary Approach*, edited by A. Mehta (Springer, Heidelberg, 1994), p. 35.

[2] H. J. Herrmann, in *3rd Granada Lectures in Computational Physics*, edited by P. L. Garrido and J. Marro (Springer, Heidelberg, 1995), p. 67.

[3] H. M. Jaeger, S. R. Nagel, and R. P. Behringer, *Rev. Mod. Phys.* **68**, 1259 (1996).

[4] L. P. Kadanoff, *Rev. Mod. Phys.* **71**, 435 (1999).

[5] O. R. Walton, in *Mechanics of Granular Materials*, edited by J. T. Jenkins and M. Satake (Elsevier, Amsterdam, 1983), p. 327.

[6] D. Hirshfeld and D. C. Rapaport, *Phys. Rev. E* **56**, 2012 (1997).

[7] A. Rosato, K. J. Strandburg, F. Prinz, and R. H. Swendsen, *Phys. Rev. Lett.* **58**, 1038 (1987).

[8] J. A. C. Gallas, H. J. Herrmann, T. Pöschel, and S. Sokolowski, *J. Stat. Phys.* **82**, 443 (1996).

[9] D. C. Rapaport, *Phys. Rev. E* **64**, 061304 (2001).

[10] F. Cantelaube and D. Bideau, *Europhys. Lett.* **30**, 133 (1995).

[11] O. Zik, D. Levine, S. G. Lipson, S. Shtrikman, and J. Stavans, *Phys. Rev. Lett.* **73**, 644 (1994).

[12] D. C. Rapaport, *Phys. Rev. E* **65**, 061306 (2002).

[13] K. M. Hill, A. Caprihan, and J. Kakalios, *Phys. Rev. Lett.* **78**, 50 (1997).

[14] K. M. Hill, A. Caprihan, and J. Kakalios, *Phys. Rev. E* **56**, 4386 (1997).

[15] M. Nakagawa, S. A. Altobelli, A. Caprihan, and E. Fukushima, *Chem. Eng. Sci.* **52**, 4423 (1997).

[16] V. Frette and J. Stavans, *Phys. Rev. E* **56**, 6981 (1997).

[17] K. Choo, T. C. A. Molteno, and S. W. Morris, *Phys. Rev. Lett.* **79**, 2975 (1997).

[18] K. Choo, M. W. Baker, T. C. A. Molteno, and S. W. Morris, *Phys. Rev. E* **58**, 6115 (1998).

[19] J. Stavans, *J. Stat. Phys.* **93**, 467 (1998).

[20] S. J. Fiedor and J. M. Ottino, *Phys. Rev. Lett.* **91**, 244301 (2003).

[21] T. Arndt, T. Siegmann-Hegerfeld, S. J. Fiedor, J. M. Ottino, and R. M. Lueptow, *Phys. Rev. E* **71**, 011306 (2005).

[22] T. Finger, A. Voigt, J. Stadler, H. G. Niessen, L. Naji, and R. Stannarius, *Phys. Rev. E* **74**, 031312 (2006).

[23] M. Newey, J. Ozik, S. M. van der Meer, E. Ott, and W. Losert, *Europhys. Lett.* **66**, 205 (2004).

[24] A. Alexander, F. J. Muzzio, and T. Shinbrot, *Gran. Matter* **5**, 171 (2004).

[25] C. R. J. Charles, Z. S. Khan, and S. W. Morris, *Gran. Matter* **8**, 1 (2006).

[26] I. S. Aranson, L. S. Tsimring, and V. M. Vinokur, *Phys. Rev. E* **60**, 1975 (1999).

[27] Z. S. Khan, W. A. Tokaruk, and S. W. Morris, *Europhys. Lett.* **66**, 212 (2004).

[28] T. Yanagita, *Phys. Rev. Lett.* **82**, 3488 (1999).

[29] S. Shiochi, *Mod. Phys. Lett. B* **12**, 115 (1998).

[30] N. Taberlet, W. Losert, and P. Richard, *Europhys. Lett.* **68**, 522 (2004).

[31] C. M. Dury and G. H. Ristow, *J. Phys. I (France)* **7**, 737 (1997).

[32] P. A. Cundall and O. D. L. Strack, *Géotechnique* **29**, 47 (1979).

[33] P. K. Haff and B. T. Werner, *Powder Tech.* **48**, 239 (1986).

[34] J. Schäfer, S. Dippel, and D. E. Wolf, *J. Phys. I (France)* **6**, 5 (1996).

[35] L. E. Silbert, D. Ertas, G. S. Grest, T. C. Halsey, D. Levine, and S. J. Plimpton, *Phys. Rev. E* **64**, 051302 (2001).

[36] D. C. Rapaport, *The Art of Molecular Dynamics Simulation* (Cambridge University Press, Cambridge, 2004), 2nd ed.

[37] G. H. Ristow and M. Nakagawa, *Phys. Rev. E* **59**, 2044 (1999).

[38] D. Levine, *Chaos* **9**, 573 (1999).

[39] S. Chandrasekhar, *Hydrodynamic and Hydromagnetic Stability* (Oxford University Press, Oxford, 1961).